



HAL
open science

Photo-induced thermal radiation of optical interference coatings submitted to a spatio-temporal illumination

P. Rouquette, C. Amra, M. Zerrad, C. Grèzes-Besset, H. Krol

► To cite this version:

P. Rouquette, C. Amra, M. Zerrad, C. Grèzes-Besset, H. Krol. Photo-induced thermal radiation of optical interference coatings submitted to a spatio-temporal illumination. *Optics Express*, 2023, 31 (22), pp.35431-35452. 10.1364/OE.495500 . hal-04235251

HAL Id: hal-04235251

<https://hal.science/hal-04235251v1>

Submitted on 1 Feb 2024

HAL is a multi-disciplinary open access archive for the deposit and dissemination of scientific research documents, whether they are published or not. The documents may come from teaching and research institutions in France or abroad, or from public or private research centers.

L'archive ouverte pluridisciplinaire **HAL**, est destinée au dépôt et à la diffusion de documents scientifiques de niveau recherche, publiés ou non, émanant des établissements d'enseignement et de recherche français ou étrangers, des laboratoires publics ou privés.

Copyright



Photo-induced thermal radiation of optical interference coatings submitted to a spatio-temporal illumination

P. ROUQUETTE,^{1,2,*}  C. AMRA,¹  M. ZERRAD,¹ 
C. GRÈZES-BESSET,² AND H. KROL²

¹Aix Marseille University, CNRS, Centrale Marseille, Institut Fresnel, Faculty of Sciences - Campus Saint Jérôme, Avenue Escadrille Normandie-Niemen, 13397 Marseille, France

²CILAS, 600 avenue de La Roche Fourcade, Pôle Alpha-Sud, 13400 Aubagne, France

*paul.rouquette@fresnel.fr

Abstract: We present an electromagnetic model for photo-induced thermal radiation in multi-layer interference filters subjected to arbitrary pulsed illumination with limited beam size. Numerical calculation is used to analyze various structures affecting thermal radiation, such as multi-dielectric mirrors in the mid-infrared range. Other zero-admittance structures are shown to strongly confine and enhance the thermal radiation with an emissivity close to unity at pre-defined frequencies (wavelength and angles). Calculation tools are chosen that encourage the use of techniques for synthesizing thin-film multilayers able to control thermal radiation.

© 2023 Optica Publishing Group under the terms of the [Optica Open Access Publishing Agreement](#)

1. Introduction

Optical interference filters are used in most areas of modern optics, because they allow to modify the parameters governing the propagation and transport of light in high-precision optical systems: reflection, transmission, absorption, phase and polarization, pulse duration, and so on [1–4]. These optical properties are thus controlled as a function of wavelength, angle of incidence and polarization. For example, today we synthesize and manufacture a multitude of optical functions such as anti-reflectors, polarizers and beam splitters, dichroic filters, mirrors and narrow-band filters, multi-pic filters, high and low pass filters, inverse filters, chirped filters and others. Synthesis (or design, or inverse problem) techniques have progressed considerably from a mathematical and algorithmic point of view, to the point where one can now synthesize any arbitrary optical (intensity) function with a multilayer. At the same time, manufacturing technologies have evolved considerably, so that one can now produce filters with several hundred thin layers of different materials, each layer ranging in thickness from a few nm to several hundred nm. Certain questions naturally remain open, such as (among others) phase and broad-band properties, large pieces and micro-substrates, and non-optical properties.

For flagship applications such as the detection of gravitational waves [5,6], or mirrors for gyro-lasers, and space optics, a current challenge is to break the ppm barrier, i.e. to ensure that total losses by absorption and scattering are less than 1 millionth of the incident flux. This state of the art has not yet been achieved, despite the low imaginary indices (a few 10^{-6}) and low roughness (a fraction of a nm) in multilayer components. It should be noted that these losses are also directly linked to the laser flux resistance of the components, depending on the illumination regime [7]. It is in this last context of very low optical losses that this work has been carried out. At the level of precision required, we need to analyze the details of the absorption mechanisms, bearing in mind that this absorption is transferred to the processes of thermal conduction, convection and radiation. Analysis of this photo-induced thermal radiation [8–10] is essential for several reasons: firstly, it enables us to trace very low levels of absorption (which are currently highly difficult to measure below 10^{-6}), and this may allow to determine the

slight imaginary indices of thin films. Secondly, it is essential to know how thermal radiation is superimposed on (or even masks) other useful communication signals. Finally, for other specific defense or energy applications, there is a huge motivation to control the amplitude, direction and wavelength of the thermal radiation. A great deal of work has been devoted to this objective using diffraction gratings, meta-surfaces and photonic crystals [11–16]; in this article we show how multilayer interference systems may notably contribute to this. The starting point is a theoretical model that is as complete as possible, operating in 4 dimensions (3 for space, 1 for time) in a spatio-temporal regime, and allowing to design maximum emissivity at predefined wavelengths.

In contrast to studies of temperature in multi-layer interference filters, thermal radiation [8–10] in such coatings has been less studied [11–13,15,17]. For applications involving energy or defense, the ability to design the angular or spectral distribution of this radiation remains a topical issue. This made it possible to create selective solar absorbers [18] or radiative coolers [19] which are components with outstanding energy-saving characteristics. Within this field we find series of work involving diffraction gratings, meta-surfaces or metamaterials [14,20–22], and multi-layers [11,23–26]. Finally, we can use this radiation to examine the components from which it originates, with the aim of extracting temperature, thermal and optical parameters, and indeed the component's structure. A recent example of thin film absorption measurements based on this signal is highlighted in [27]. We have also to mention the work on optical sources created with thermal radiation [14].

Several pieces of theoretical and experimental work [11–13,17,28] have been devoted to studying thermal emission in multi-layer systems (sometimes known in the community as photonic crystals). The solution method is moderately complex for a component at thermodynamic equilibrium (uniform temperature within the component). On the other hand, the complexity of the model increases for photo-induced emission, where the source of heat comes from the absorption of an optical beam on which spatio-temporal variations have been imposed [29]. In this context, a first difficulty is related to the conditions of application of the fluctuation-dissipation theorem (FDT), in that the temperature itself undergoes spatio-temporal variations, determined, most often, in the case of quasi-unidirectional and quasi-monochromatic illumination. The imaginary indices of thin-film materials (dielectric or metallic) are then responsible for the absorption A within the volume of the multi-layer component, whose depth-wise distribution $\frac{dA}{dz}(z)$ creates the temperature $T(z)$. This temperature then feeds the bulk thermal radiation sources in each of the layers in the stack. Certain methods are based on a so-called indirect technique that, for each temporal and spatial frequency, consists in identifying the absorption with the emissivity [11,30]. Direct methods also exist based on solving Maxwell's equations in the presence of thermal currents [11–13,17,31,32], making use in particular of dyadic Green's functions. Absorption resulting from transient (pulsed) illumination is less frequently considered.

Hence this article is devoted to the theoretical and numerical study of photo-induced thermal radiation in optical multi-layers [1,4] currently used to filter light (mirrors and filters, splitters and polarizers, anti-reflection layers and absorbers, etc.). More precisely, this is photo-induced thermal radiation, i.e. created by the absorption of the component under arbitrary spatio-temporal illumination. We take account of the (2D) spatial form of the incident beam, so that we can accurately describe the 3D thermal diffusion processes within the stack [29]. From a temporal point of view, our interest is in a quasi-monochromatic pulsed ($>ps$) illumination. The thermal radiation which results therefore displays temporal, angular (normal and azimuthal), and spectral behavior that depends on the opto-geometric formula of the interference filter (thicknesses and complex indices, alternating materials) and on the characteristics of the incident beam (energy, pulse duration, polarization, spot size).

This work follows a recent article [29] in which we calculate the temperature from the classical heat equation, which is an essential step before considering thermal radiation. The temperature calculation was made based on an analogy between optical propagation and thermal diffusion

[33], allowing the same tools to be used (complex admittances and effective indices) to solve the optical and thermal equations. Now concerning thermal radiation, the model is also essentially analytical in the sense that we are solving Maxwell's equations in the presence of bulk currents (electric and magnetic) in each layer of the stack; recall that the radiation originates from these currents (which depend on temperature), in accordance with the FDT [8–10,30–32,34]. Having established an expression for these currents, the method of solution is similar (although more complex) to that which we developed for calculating bulk scattering [35] or luminescent micro-cavities in multi-layer systems [4,36,37]. Thus, we make use of a double Fourier Transform (FT) of Maxwell's equations, essentially considering spatio-frequential wave packets, for which the unknowns are the amplitude distributions. Note that this approach is essential not only for the radiation that emerges out of the component to propagate into free space, but also for the evanescent waves that remain confined within the immediate neighborhood of the component and may be decoupled by an optical tunneling effect [38], as well as for the thermal radiation which is transferred to the guided modes of the multi-layer structure [4,39]. Furthermore, radiation is calculated here for the transient regime, in response to a single or repeated laser pulse. These remarks explain why the classical (indirect) method is not used, which consists of linking the value of the radiation (or emissivity) with a calculation of the monochromatic unidirectional absorption [11,30]. Finally, the model and its implementation allow temporal, angular or wavelength diagrams of the thermal radiation to be predicted for various transient illumination regimes. In general, computational tools have been chosen to highlight the design techniques of multi-layer systems. This allows us to emphasize certain structures that strongly confine and enhance thermal radiation in narrow bandwidths, with an emissivity close to unity at pre-defined frequencies.

The paper is structured as follows: in section 2 the field and flux radiated by the thermal currents is calculated, while sections 3 and 4 are devoted to numerical calculation. For a better reading, the details of the calculations are reported in the supplement and only the main steps are mentioned in section 2. Section 3 shows how a multi-dielectric mirror can have a profound effect on the spectral distribution of the radiation. In section 4, specific ZAL [4,40] structures are used to obtain an intense confinement and enhancement of the radiation. The conclusion is given in section 5.

2. Calculation of the electromagnetic field radiated by the currents responsible for thermal radiation

An essential first step is to introduce into Maxwell's equations the bulk currents, electrical and magnetic, that are responsible for thermal radiation. This step is based directly on the fluctuation-dissipation theorem (FDT) from statistical or quantum physics [9,34,41,42]. In section 1 of Supplement 1, we first review this theorem in canonical form, and then use it to retrieve an analytical expression for the electrical and magnetic bulk currents in each layer of the stack. This approach leads to a coherent exposition consistent with the framework of classical electromagnetism, and can thus draw on our previous theoretical and numerical work on bulk scattering in multi-layer systems [35].

2.1. Analytical expression of the thermal currents

Following the Supplement 1, the temporal Fourier transform of the electric $\tilde{J}_{u,i}$ and magnetic $\tilde{M}_{u,i}$ currents responsible for thermal radiation follow, with $u = x, y$ or z :

$$\sqrt{\delta V} \tilde{J}_{u,i}(f, \vec{r}, z) = e^{j\varphi_{u,i}^J(f, \vec{r}, z)} \sqrt{4\pi f} \Theta[2\pi f, T_i(\vec{r}, z)] \text{Im}[\tilde{\epsilon}_i(f)] \quad (1)$$

$$\sqrt{\delta V} \tilde{M}_{u,i}(f, \vec{r}, z) = e^{j\varphi_{u,i}^M(f, \vec{r}, z)} \sqrt{4\pi f} \Theta[2\pi f, T_i(\vec{r}, z)] \text{Im}[\tilde{\mu}_i(f)] \quad (2)$$

with:

$$\Theta(\omega, T) = \frac{\bar{h}\omega}{e^{\frac{\bar{h}\omega}{k_B T}} - 1} \quad (3)$$

where \bar{h} and k_B are the reduced Planck and Boltzmann constants, respectively. In these relations the spectral phases of the currents (or the arguments of their FTs) are denoted φ_u^J and φ_u^M , the temperature in layer (i) is $T_i(\vec{r}, z)$, the space coordinates (see Fig. 1) is $(\vec{r}, z) = (x, y, z)$ and f is the temporal frequency. The temporal Fourier transforms of permittivity and permeability in layer (i) are denoted $\tilde{\varepsilon}_i$ and $\tilde{\mu}_i$. Relation (1) and (2) are given for the analytical expressions of the thermal currents generated by an elementary volume δV . We will see further (section 2.6) how the assumption as to the statistical nature of the spectral phases (independence, uniform distributions) allows the introduction of Dirac distributions and simplification of the calculations at various stages. Note also that the FDT is generally used at thermodynamic equilibrium, and that its justification in a spatio-temporal temperature distribution is discussed in the Supplement 1.

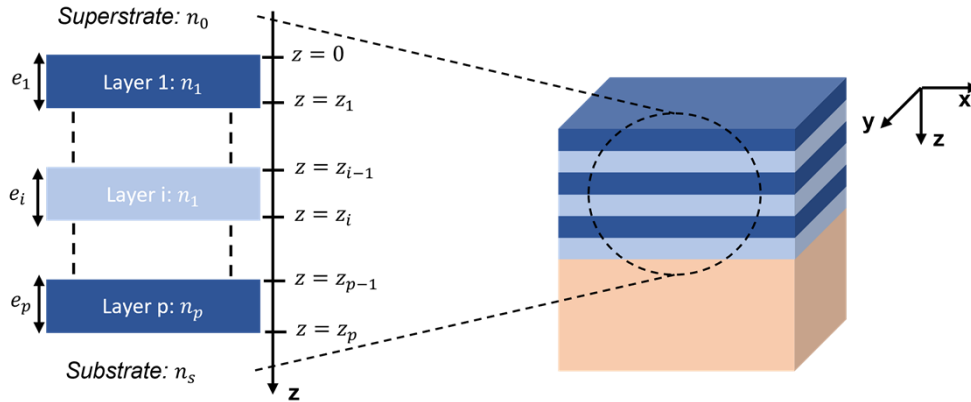


Fig. 1. General structure of a planar multilayer stack.

At this stage the problem is well posed, and we can turn to solving Maxwell's equations in the presence of bulk electric and magnetic currents in each of the layers of the interference filter. This observation means that we can proceed to a method of solution similar to that already used for bulk scattering [35] and which we now detail.

2.2. Calculating the electromagnetic field in a multi-layer system

Figure 1 shows the geometry of the multi-layer system under investigation. We start by recalling the main results of calculating the stationary electric field in a multi-layer interference filter, and to that end we draw primarily on the work described in [4]. The interference filter is formed from p layers, each comprising a linear, homogeneous, isotropic and uncharged medium. For each layer i , the complex optical index is n_i and its thickness e_i .

Calculation of the electromagnetic field in the component requires a double Fourier transform (FT) with respect to time t and to transverse space variable $\vec{r} = (x, y)$. Hence, we consider the decomposition of the field in the form of spatial and frequency packets. The temporal FT (in the first Fourier plane) is defined as follows:

$$\tilde{X}_i(f, \vec{r}, z) = \int_t X_i(t, \vec{r}, z) e^{j2\pi f t} df \Leftrightarrow X_i(t, \vec{r}, z) = \int_f \tilde{X}_i(f, \vec{r}, z) e^{-j2\pi f t} df \quad (4)$$

where X_i denotes the electric field E_i in medium i or the magnetic field H_i , and f is the temporal frequency, the conjugate Fourier variable of time t .

The spatial FT (in the second Fourier plane) is defined as:

$$\hat{X}_i(f, \vec{\nu}, z) = \int_{\vec{r}} \tilde{X}_i(f, \vec{r}, z) e^{-j2\pi\vec{\nu}\cdot\vec{r}} d\vec{r} \Leftrightarrow \tilde{X}_i(f, \vec{r}, z) = \int_{\vec{\nu}} \hat{X}_i(f, \vec{\nu}, z) e^{j2\pi\vec{\nu}\cdot\vec{r}} d\vec{\nu} \quad (5)$$

where $\vec{\nu}$ is the spatial frequency, the conjugate Fourier variable of transverse space \vec{r} . This FT enables positive optical paths to be obtained.

In the second Fourier plane, where the field is monochromatic and unidirectional, we can [4] make use of the concept of complex admittance $Y(f, \nu, z)$. This variable depends on the polarization and on the whole multi-layer, and links the tangential electric and magnetic fields (stationary or progressive/retrograde) in the following manner [4]:

$$\vec{H}_i(f, \vec{\nu}, z) = Y_i(f, \nu, z) \vec{z} \wedge \vec{E}_i(f, \vec{\nu}, z) \quad (6)$$

Since these tangential fields are continuous in the presence of bulk currents, the admittance Y_i is also continuous in the stack. Let $X_i(z = z_i) = X_i$ and $Y_i(z = z_i) = Y_i$ be the electromagnetic field and complex admittance in layer i at interface i .

Within the emergent media (substrate or superstrate), the field is progressive or retrograde, such that the admittance is identified with the effective index $\tilde{n}_i(f, \nu)$ given by [4]:

$$\tilde{n}_i = \begin{cases} \frac{1}{\eta_0 \mu_{r,i}} \frac{n_i \alpha_i}{k_i} & \text{in S polarization} \\ \frac{1}{\eta_0 \mu_{r,i}} \frac{n_i k_i}{\alpha_i} & \text{in P polarization} \end{cases} \quad (7)$$

where $\eta_0 = \sqrt{\mu_0/\epsilon_0}$ is the impedance of free space in vacuo, $\mu_{r,i}$ is the relative permeability of medium i and $\alpha_i = \sqrt{k_i^2 - (2\pi\nu)^2}$, with wavenumber $k_i = 2\pi n_i/\lambda$ and λ the wavelength.

Consequently, admittances are calculated by recurrence [4], either from their initial value $-\tilde{n}_0$ in the superstrate (denoting the admittances as Y'_i) or from their initial value \tilde{n}_s in the substrate (denoting the admittances as Y_i). Knowing these admittances, we can then describe the variation of the electromagnetic field over the entire depth of the stack, given that the field is known at height z ; the latter datum is given by the boundary conditions in the presence of currents, as detailed in section 2.4.

At this stage we recall that the use of a double FT combined with complex admittances is well suited to the problem, and we have already used this for the calculation of surface [4] and volume [35] scattering, luminescent micro-cavity [4,36,37] and temperature [29,33] in multi-layer structures.

Finally, note that the radiation flux through a plane at altitude z can be expressed uniquely using the tangential components of the electromagnetic field. Hence, unless otherwise stated, all the fields considered in the rest of this document are tangential fields.

2.3. Thermal radiation flux

The instantaneous real Poynting flux through a plane of normal \vec{z} at altitude z outside the multilayer classically writes as [4]:

$$\Phi(t) = \int \{ [\vec{E}(t, \vec{r}, z) \wedge \vec{H}(t, \vec{r}, z)] \cdot \vec{z} \} d\vec{r} \quad (8)$$

Note that this formula involves the fields of the time domain, for which reason the flux is time dependent. Furthermore, it does not depend on the \vec{r} variable, since it is a global flux across a plane. Also, for transparent media it does not depend on the z altitude. As far as the response times of the optical detectors are concerned, which are very long compared with the

temporal period of the thermal radiation being considered (our application will be limited to the visible and infra-red spectral domain), these detectors behave as low pass filters [4]. Under these conditions the (multi-spectral) polychromatic flux can be written as the sum of monochromatic fluxes [4]. This property means that we can avoid the *a priori* introduction of Dirac distributions $\delta(f - f')$ in the currents [10]. Hence in the far field we obtain for the density per unit area of the polychromatic flux through an infinite plane of normal \vec{z} , the following expression [4,8,10]:

$$\frac{d\Phi}{dS} = 4 \int_{f=0}^{+\infty} \Re\{\Pi \cdot \vec{z}\} df \tag{9}$$

where $\Pi = \frac{1}{2} \vec{E}^*(\vec{r}, z, f) \wedge \vec{H}(\vec{r}, z, f)$ is the complex Poynting vector in the harmonic regime (first Fourier plane), and (\vec{E}, \vec{H}) are the tangential electromagnetic fields induced by the bulk densities of the thermal currents (1) and (2). Observe that calculating the flux density per unit area in the end media requires that we consider the field (\vec{E}_0, \vec{H}_0) and the normal $\vec{n} = -\vec{z}$ for the superstrate, as well as the field (\vec{E}_s, \vec{H}_s) and the normal $\vec{n} = \vec{z}$ for the substrate. Note also in Expression (9) that the flux density is no more time dependent, since it is a frequency integral involving fields of the first Fourier plane. This flux density is given for the far field through a plane at altitude z [4].

Expression (9) is given for the flux density emitted in all directions of space at all wavelengths. If we now turn our attention to the monochromatic flux radiated in a single direction in the far field, we have to consider the double spectral flux density (monochromatic, unidirectional) in the end media, assumed transparent [4]. Putting $\partial\vec{v} = \partial v_x \partial v_y$, and now using the double FT (spatial and temporal) of the fields $(\vec{E}_0$ and $\vec{E}_s)$ in the second Fourier plane, we get [4]:

$$\begin{aligned} \frac{\partial\Phi_0}{\partial f \partial\vec{v}} &= 2 \Re\{\tilde{n}_0(v, f)\} |\vec{E}_0(\vec{v}, f)|^2 \\ \frac{\partial\Phi_s}{\partial f \partial\vec{v}} &= 2 \Re\{\tilde{n}_s(v, f)\} |\vec{E}_s(\vec{v}, f)|^2 \end{aligned} \tag{10}$$

with the spatial frequency $\vec{v} = v(\cos \phi, \sin \phi)$, $v = |\vec{v}| = n_0 \sin \theta_0 / \lambda$, and where (θ_0, ϕ) denotes the spherical coordinate angles defined in the superstrate and substrate respectively (see Supplement 1, Fig. S1). Relation (10) expresses the flux per unit of spatial frequencies in terms of the double Fourier transform of the fields. It relates to the energy carried out in the far field at one direction. As expected, it does not depend on the space variables. Note that the flux carried by evanescent waves is zero for transparent media, since for these high-frequency waves we have $\Re\{\tilde{n}_i(v, f)\} = 0$ [4]. Also, we observe in relation (10) that \vec{E}_0 and \vec{E}_s are respectively retrograde (travelling in the $-\vec{z}$ direction) and progressive (\vec{z} direction) in the emergent media, and that the flux densities are polarization dependent at this step.

Looking a bit more deeply, consider the field produced by layer i on interface j , written \vec{E}_{ij} . This field results from the bulk density of thermal currents within layer i . According to the superposition theorem, the total field on an interface is therefore the sum of the contributions of each layer. Hence, we can write

$$\vec{E}_j = \sum_{i=1}^p \vec{E}_{ij} \tag{11}$$

Now let us express this field at the end interfaces (0 and p) of the component, involving only the fields ($\vec{E}_{i,i-1}$, \vec{E}_{ii}) created by volume i at interfaces (i - 1) and (i) delimiting this volume:

$$\begin{aligned} \vec{E}_0 &= \sum_{i=1}^p \vec{E}_{i0} = \sum_{i=1}^p C'_{i-1,0} \vec{E}_{i,i-1} \\ \vec{E}_p &= \sum_{i=1}^p \vec{E}_{ip} = \sum_{i=1}^p C_{ip} \vec{E}_{ii} \end{aligned} \tag{12}$$

where the transfer coefficients are given by [4]:

$$\begin{aligned} C'_{0,i-1} &= \begin{cases} 1 & \text{if } i = 1 \\ \prod_{k=i-1}^1 \left(\cos \delta_k + j \frac{Y'_{k-1}}{\tilde{n}_k} \sin \delta_k \right) & \text{else} \end{cases} \\ C_{pi} &= \begin{cases} 1 & \text{if } i = p \\ \prod_{k=i+1}^p \left(\cos \delta_k - j \frac{Y_k}{\tilde{n}_k} \sin \delta_k \right) & \text{else} \end{cases} \end{aligned} \tag{13}$$

where $\delta_k = \alpha_k e_k$ with e_k the thickness of layer k and Y_k, Y'_k the complex admittances at interface k, calculated from the substrate and superstrate respectively [4].

The rest of the calculation involves introducing Expression (12) into (10), which equates to considering the modulus squared of the sum of the fields ($\vec{E}_{i,i-1}$, \vec{E}_{ii}) weighted by the transfer coefficients ($C'_{0,i-1}$, C_{pi}). This throws up cross terms $\vec{E}_{i0} \vec{E}_{j0}^*$ or $\vec{E}_{ip} \vec{E}_{jp}^*$ characteristic of interference between the fields emitted by layers i and j, where $i \neq j$. In the more general case, we can introduce at this stage the concept of mutual coherence between fields or currents [37]. However, as indicated in section 2.1, for these thermal cases the phases (ψ_i, ψ_j) of the currents creating (\vec{E}_{i0} , \vec{E}_{j0}^*) or (\vec{E}_{ip} , \vec{E}_{jp}^*) are assumed to be independent and uniformly distributed, such that these terms will disappear for $i \neq j$ if integrated over any solid angle of detection (characteristic of receiver aperture).

Consequently, for our application the double spectral flux density causes only quadratic terms to appear, in the form:

$$\begin{aligned} \frac{\partial \Phi_0}{\partial f \partial \vec{v}} &= 2\Re \{ \tilde{n}_0(v, f) \} \sum_{i=1}^p |C'_{i-1,0}(v, f)|^2 |\vec{E}_{i,i-1}(\vec{v}, f)|^2 \\ \frac{\partial \Phi_s}{\partial f \partial \vec{v}} &= 2\Re \{ \tilde{n}_s(v, f) \} \sum_{i=1}^p |C_{ip}(v, f)|^2 |\vec{E}_{ii}(\vec{v}, f)|^2 \end{aligned} \tag{14}$$

Now it remains only to express the electromagnetic field created by the thermal current in layer i on its upper interface ($\vec{E}_{i,i-1}$) or lower interface (\vec{E}_{ii}).

2.4. Limitation to non-magnetic materials

Since most materials used in optical interference coatings are non-magnetic ($\mu''_i = 0$), we will consider that the magnetic thermal current is zero, thus reducing the number of terms to be calculated. Hence, we must determine the field resulting from bulk densities of electric current given by (1) in a multi-layer system. This calculation of the electromagnetic field created by an arbitrary bulk density of electric current in a multi-layer component is given in [35]. Recall here

the expression for the field created by current (i) on the upper interface ($z = z_i$) and the lower interface ($z = z_{i-1}$) of layer i of thickness e_i , i.e.

$$\begin{aligned}\vec{E}_{i,i-1} &= \frac{1}{\Delta Y_{i-1}} \left[F_{1i} \vec{E}_i^g(z_i) + F_{2i} \vec{z} \wedge \vec{H}_i^g(z_i) + F_{3i} \vec{E}_i^g(z_{i-1}) + F_{4i} \vec{z} \wedge \vec{H}_i^g(z_{i-1}) \right] \\ \vec{E}_{ii} &= \frac{1}{\Delta Y_i} \left[F_{5i} \vec{E}_i^g(z_i) + F_{6i} \vec{z} \wedge \vec{H}_i^g(z_i) + F_{7i} \vec{E}_i^g(z_{i-1}) + F_{8i} \vec{z} \wedge \vec{H}_i^g(z_{i-1}) \right]\end{aligned}\quad (15)$$

In this expression, the presence of the term in $1/\Delta Y_j$, where $\Delta Y_j = Y_j - Y'_j$ is the difference in admittance from each side of interface i, recalls the possibility of exaltation or inhibition of the radiation, in relation to the structure of the multi-layer [4,36,37,40,43]. This property will be used in section 4. The other coefficients are given by

$$\begin{aligned}F_{1i} &= -j\tilde{n}_i \sin \delta_i - Y_{i-1} \cos \delta_i; F_{2i} = -\cos \delta_i - j\frac{Y_{i-1}}{\tilde{n}_i} \sin \delta_i; F_{3i} = Y_{i-1}; F_{4i} = 1 \\ F_{5i} &= -Y'_i; F_{6i} = -1; F_{7i} = -j\tilde{n}_i \sin \delta_i + Y'_i \cos \delta_i; F_{8i} = \cos \delta_i - j\frac{Y'_i}{\tilde{n}_i} \sin \delta_i\end{aligned}\quad (16)$$

In Eq. (15) note also that the field $(\vec{E}_i^g, \vec{H}_i^g)$ is a particular solution of the Helmholtz equation in the second Fourier plane, resulting from the source term \vec{S} corresponding to the electric current in layer (i). This tangential field is a result of the convolution product of the space variable z between the source term and the Green's function associated with the Helmholtz equation. Hence in the second Fourier plane we have [35]

$$\vec{X}_i^g = G_i *_{z} \vec{S}^{X_i} \quad \text{with} \quad G_i = \frac{1}{2j\alpha_i} e^{j\alpha_i|z|}\quad (17)$$

where $X_i = E_i$ or H_i ; and in the first Fourier plane,

$$\begin{aligned}\vec{S}^{E_i} &= -j\omega\mu_i \vec{J}_i + \frac{1}{j\omega\epsilon_i} \overrightarrow{\text{grad}}[\text{div} \vec{J}_i] \\ \vec{S}^{H_i} &= -\overrightarrow{\text{curl}}[\vec{J}_i]\end{aligned}\quad (18)$$

Note that we have not used the dyadic Green's function but have solved the Helmholtz equation in the second Fourier plane in the presence of sources. The analytical calculation of the source terms is slightly more complex, but this choice enables us to draw on our method of calculation for bulk scattering [35]. As a result, we need to expand on the calculation of the spatial FTs for the source terms given in Eq. (18). We find:

$$\vec{S}^{E_i} = -j\omega\mu_i \left(\begin{aligned} &\left(1 - \frac{\sigma_x^2}{k_i^2}\right) \hat{J}_{x,i} - \frac{\sigma_x\sigma_y}{k_i^2} \hat{J}_{y,i} + j\frac{\sigma_x}{k_i^2} \frac{\partial \hat{J}_{z,i}}{\partial z} \\ &-\frac{\sigma_x\sigma_y}{k_i^2} \hat{J}_{x,i} + \left(1 - \frac{\sigma_y^2}{k_i^2}\right) \hat{J}_{y,i} + j\frac{\sigma_y}{k_i^2} \frac{\partial \hat{J}_{z,i}}{\partial z} \end{aligned} \right)\quad (19)$$

and

$$\vec{S}^{H_i} = \left(\begin{aligned} &\frac{\partial \hat{J}_{y,i}}{\partial z} - j\sigma_y \hat{J}_{z,i} \\ &-\frac{\partial \hat{J}_{x,i}}{\partial z} + j\sigma_x \hat{J}_{z,i} \end{aligned} \right)\quad (20)$$

Hence, using Eq. (17), the expressions for the electrical (19) and magnetic (20) source terms allow us to obtain values for the particular solutions $(\vec{E}_i^g, \vec{H}_i^g)$ at the interfaces ($i-1$ and i) that appear in Expression (15). This provides the tangential electric field on the upper and lower interfaces of layer i. Before expanding any further on these particular solutions (section 2.6), it is important to return to the calculation in Eq. (14) to take account of the polarization of the wave emitted in one direction.

2.5. Taking account of polarization

Appearing in the expression for the thermal radiation flux (Eq. (14)) are the coefficients \tilde{n} and C which depend on light polarization. To calculate these coefficients, we need to know the wave polarization with respect to a reference plane (\vec{v}, \vec{z}) , which allows to define the amount of light that would be measured after passing through an analyzer. $|\vec{E}_{ii-1}|^2$ and $|\vec{E}_{ii}|^2$ must therefore be calculated by distinguishing the S polarization (or TE) from the P polarization (or TM). This leads us to address polarization effects in detail, which is done in section 2 of Supplement 1. It is shown that the modulus squared of the electric field produced by layer i on its lower interface, denoted $|\vec{E}_{i,i-1}|^2$, is a linear combination of $|\hat{E}_{x,i,i-1}|^2$, $|\hat{E}_{y,i,i-1}|^2$ and $\Re\{\hat{E}_{x,ii-1}\hat{E}_{y,ii-1}^*\}$. In accordance with (15), these terms are themselves a linear combination of Hermitian products of the particular solutions $(\vec{E}_i^g, \vec{H}_i^g)$ at interfaces $(i - 1$ and $i)$. Finally, in accordance with Eqs. (19) and (20), these particular solutions can be expressed as a convolution product between the Green's function and a source term, given as a linear combination of the current components on the axes. Consequently, the radiation flux produced by a layer (i) is a linear combination of elementary fluxes, written $\Phi_{i,a,b}^{el}$, whose spectral densities can be written for each polarization as:

$$\forall a, b \in \{x, y, z\}, \quad \frac{\partial \Phi_{i,a,b}^{el}}{\partial f \partial \vec{v}}(\vec{v}) = \int_{z'} \int_{z''} L_i(v, z', z'') \hat{J}_{a,i}^*(\vec{v}, z') \hat{J}_{b,i}(\vec{v}, z'') dz'' dz' \quad (21)$$

In Expression (21), the domain of integration of z' and z'' is that of layer i , i.e. $[z_{i-1}, z_i]$. The current terms will finally be given by the FDT, to be covered in section 2.6.

2.6. Using the random phase nature of thermal currents and the dissipation fluctuation theorem

In order to develop Relation (21) we return to the expression for the thermal current given in (1), written in the following synthetic form:

$$\forall a \in \{x, y, z\}, \quad \hat{J}_{a,i}(\vec{v}, z) = |\hat{J}_{a,i}(\vec{v}, z)| e^{j\psi_{a,i}(\vec{v}, z)} \quad (22)$$

Since the phase terms are independent and uniformly distributed, we can write

$$\frac{\partial \Phi_{i,a,b}^{el}}{\partial f \partial \vec{v}}(\vec{v}) = 0 \text{ if } a \neq b \quad (23)$$

such that the case for $a \neq b$ is no longer considered. Note that this behavior is generally considered by the introduction of Kronecker delta symbols into the FDT [8,10,32]. We now introduce the phase terms into Eq. (21) :

$$\frac{\partial \Phi_{i,a,a}^{el}}{\partial f \partial \vec{v}}(\vec{v}) = \int_{z'} \int_{z''} L_i(v, z', z'') |\hat{J}_{a,i}(\vec{v}, z')| |\hat{J}_{a,i}(\vec{v}, z'')| e^{j(\psi_{a,i}(\vec{v}, z'') - \psi_{a,i}(\vec{v}, z'))} dz'' dz' \quad (24)$$

In contrast to the previous cases where the phases were independent, a phase difference appears in Eq. (24) of the same variable $\psi_{a,i}(\vec{v}, z)$ taken at 2 different heights. As a result, the quantity (Eq. (24)) is integrated only over the path defined by $z = z'$ where the phases are identical, giving

$$\frac{\partial \Phi_{i,a,a}^{el}}{\partial f \partial \vec{v}}(\vec{v}) = \int_{z'} L_i(v, z') |\hat{J}_{a,i}(\vec{v}, z')|^2 dz' \quad (25)$$

This amounts to saying that the thermal agitation at some specific height is uncorrelated with that at other heights. This behavior is generally considered into the FDT expression using a Dirac distribution over the spatial variable [8–10], so as to take account of locality.

Finally, we need to use the expression for the FDT in the first Fourier plane, in which are written the currents involved in Eq. (21). Using the definition of the inverse FT, we get

$$\frac{\partial \Phi_{i,a,a}^{el}}{\partial f \partial \vec{v}}(\vec{v}) = \int_{z'} L_i(\nu, z') \int_{\vec{r}} \int_{\vec{r}'} \tilde{J}_{a,i}^*(\vec{r}, z') \tilde{J}_{a,i}(\vec{r}', z') e^{-j2\pi(\vec{r}-\vec{r}') \cdot \vec{v}} d\vec{r}' d\vec{r} dz' \quad (26)$$

We use the same reasoning as before, namely that we can describe the bulk density of the electric current in the first Fourier plane using a phase assumed to be random, i.e.

$$\tilde{J}_{a,i}(\vec{r}, z) = |\tilde{J}_{a,i}(\vec{r}, z)| e^{j\varphi_{a,i}(\vec{r}, z)} \quad (27)$$

We proceed as before to obtain Relation (25). With the phase terms appearing in Relation (26) in the form $e^{j(\varphi_{a,i}(\vec{r}', z') - \varphi_{a,i}(\vec{r}, z))}$, this integral must be performed over the path $\vec{r} = \vec{r}'$, giving

$$\frac{\partial \Phi_{i,a,a}^{el}}{\partial f \partial \vec{v}}(\vec{v}) = \int_{z'} L_i(\nu, z') \int_{\vec{r}} |\tilde{J}_a(\vec{r}, z')|^2 d\vec{r} dz' \quad (28)$$

Finally, taking account of the current expressed in Relation (1), the double spectral density of the elementary flux radiated by the entire volume of the sample can be written in the form

$$\frac{\partial \Phi_{i,a,a}^{el}}{\partial f \partial \vec{v}}(\vec{v}) = \frac{\partial \Phi_i^{el}}{\partial f \partial \vec{v}}(\vec{v}) = 4\pi f \tilde{\epsilon}_i''(f) \int_z L_i(\nu, z) \int_{\vec{r}} \Theta(2\pi f, T_i(\vec{r}, z)) d\vec{r} dz \quad (29)$$

From a numerical point of view, we can choose an integration step Δz such that the temperature does not vary within the interval Δz . This simplifies Expression (29) since the function L_i can be integrated analytically over z . This amounts, in effect, to integrating the Green's function and its derivative. Finally, Expression (29) can be rewritten for a sub-layer k in layer i as the product of 2 integrals:

$$\frac{\partial \Phi_{i,k}^{el}}{\partial f \partial \vec{v}}(\vec{v}) = 4\pi f \tilde{\epsilon}_i''(f) \left\{ \int_{\vec{r}} \Theta(2\pi f, T_i(\vec{r}, z_{i,k})) d\vec{r} \right\} \left\{ \int_{z_{i-1}+k_i\Delta z_i}^{z_{i-1}+(k_i+1)\Delta z_i} L_i(\nu, z) dz \right\} \quad (30.a)$$

with:

$$0 \leq k_i \leq K_i - 1, \quad K_i = \frac{e_i}{\Delta z_i}, \quad z_{i,k} = z_{i-1} + k_i \Delta z_i \quad (30.b)$$

and:

$$\frac{\partial \Phi_i^{el}}{\partial f \partial \vec{v}}(\vec{v}) = \sum_{k=0}^{K_i-1} \frac{\partial \Phi_{i,k}^{el}}{\partial f \partial \vec{v}}(\vec{v}) \quad (30.c)$$

2.7. Final expression for the thermal radiation flux

The complete solution for the thermal radiation flux in the end media is detailed in section 3 of [Supplement 1](#). Summing over the total number $q = \sum_{i=1}^p K_i$ of sub-layers in the stack, the double spectral flux density can be expressed in the end media as

$$\begin{aligned} \frac{\partial \Phi_0}{\partial f \partial \vec{v}} &= 2 \sum_{i=1}^q 4\pi f \tilde{\epsilon}_i'' \Re \{ \tilde{n}_0 \} \frac{|C'_{0,i-1}|^2}{4|\tilde{n}_i|^2 |\Delta Y_{i-1}|^2} \beta_i^0(\nu, f) \left\{ \int_{\vec{r}} \Theta(2\pi f, T_i(\vec{r}, z_i)) d\vec{r} \right\} \\ \frac{\partial \Phi_S}{\partial f \partial \vec{v}} &= 2 \sum_{i=1}^q 4\pi f \tilde{\epsilon}_i'' \Re \{ \tilde{n}_s \} \frac{|C_{i,q}|^2}{4|\tilde{n}_i|^2 |\Delta Y_i|^2} \beta_i^s(\nu, f) \left\{ \int_{\vec{r}} \Theta(2\pi f, T_i(\vec{r}, z_i)) d\vec{r} \right\} \end{aligned} \quad (31)$$

where β_i^x is a function dependent on polarization and defined as

$$\beta_i^x = \begin{cases} \left(|G_{1i}^x|^2 + |G_{2i}^x|^2 \right) \frac{1-e^{-2\delta_i''}}{2\alpha_i''} + 2\Re \{ G_{1i}^x G_{2i}^{x*} \} \frac{\sin(\delta_i') e^{-\delta_i''}}{\alpha_i'} & S \text{ polarization} \\ \left(|G_{1i}^x|^2 + |G_{2i}^x|^2 \right) \frac{1-e^{-2\delta_i''}}{2\alpha_i''} \left(1 + \frac{\sigma^2}{|\alpha_i|^2} \right) + 2\Re \{ G_{1i}^x G_{2i}^{x*} \} \frac{\sin(\delta_i') e^{-\delta_i''}}{\alpha_i'} \left(1 - \frac{\sigma^2}{|\alpha_i|^2} \right) & P \text{ polarization} \end{cases} \quad (32)$$

and $G_{1i}^0 = (\tilde{n}_i - Y_{i-1}) e^{-j\delta_i}$; $G_{2i}^0 = \tilde{n}_i + Y_{i-1}$; $G_{1i}^s = \tilde{n}_i - Y_i'$ and $G_{2i}^s = (\tilde{n}_i + Y_i') e^{-j\delta_i}$.

Note in Expression (31) that the spatial integration is limited to the extent of the Θ function introduced in Expression (3). If the ambient temperature could be neglected, this extent would be limited to that of the photo-induced temperature whose lateral profile is known [29]. Otherwise the integration must be performed over the entire heated area (so as to take account of the ambient temperature).

The advantage of the expressions in (31) is that they express the radiation flux as a function of the optical variables commonly used for the design of optical interference coatings, namely complex admittances and effective indices; hence they differ from the expressions given in the literature [17]. Moreover, temperature was also calculated with these same variables using an optical-thermal analogy [33]. Recall that these expressions, associated with a knowledge of the temporal variation of the temperature field [29], enable the thermal radiation to be determined as a function of time (for a scale greater than the thermalization time).

2.8. Variables used in the numerical calculation

Here we need to define the variables to be calculated numerically, and which can be compared with the literature. Expression (31) can be expressed for a given multilayer as follows:

$$\frac{\partial \Phi}{\partial f \partial \nu} = \sum_{i=1}^q L_i'(f, \nu) \left\{ \int_{\vec{r}} \Theta(2\pi f, T_i(\vec{r}, z_i)) d\vec{r} \right\} = L^*(f, \nu) \quad (33)$$

Note at this step that L^* is a flux density per unit of spatial frequencies, which is not normalized by the emissive surface. By analogy with light scattering [4,35] and luminescent micro-cavities [4,36,37,43], it is common to consider the spectral flux density per unit solid angle [8,11], also referred to as the electromagnetic intensity. Hence, distinguishing the superstrate from the substrate and making a change of variable as described in [4], we get the intensities

$$\begin{aligned} \frac{\partial \Phi_0}{\partial \lambda \partial \Omega_0} &= L^* \left(\frac{c}{\lambda}, \frac{n_0 \sin \theta_0}{\lambda} \right) \left(\frac{k_0}{2\pi} \right)^2 \frac{c}{\lambda^2} \cos \theta_0 \\ \frac{\partial \Phi_s}{\partial \lambda \partial \Omega_s} &= L^* \left(\frac{c}{\lambda}, \frac{n_s \sin \theta_s}{\lambda} \right) \left(\frac{k_s}{\lambda} \right)^2 \frac{c}{\lambda^2} \cos \theta_s \end{aligned} \quad (34)$$

where $d\Omega_0 = \sin \theta_0 d\theta_0 d\phi$ and $d\Omega_s = \sin \theta_s d\theta_s d\phi$ are the elementary solid angles defined respectively by the angles (θ_0, ϕ) of the superstrate and (θ_s, ϕ) of the substrate (see Supplement 1, Fig. S1); $k_i = 2\pi n_i / \lambda$ is the wavenumber and c the speed of light in vacuo. The advantage of these variables is that, when normalized by the exciting radiative power, they provide the absolute value of radiation that can be measured in far field within $d\Omega$. By analogy with photometry, these variables can be related to a luminance ρ defined as [4]

$$\frac{\partial \Phi_u}{\partial \lambda \partial \Omega_u} = \rho_u \cos \theta_u \quad (35)$$

It is also common to consider the radiative spectral intensity [8] resulting from normalization by an emissive elementary area on the sample. This quantity, expressed in $\text{W} \cdot \text{m}^{-2} \cdot \text{m}^{-1} \cdot \text{sr}^{-1}$, is

defined as

$$\frac{\partial \Phi}{\partial \lambda \partial \Omega \partial S} = I(\lambda, \theta, \phi) \cos \theta \quad (36)$$

Following Expression (31) the $I(\lambda, \theta, \phi)$ terms are given, with $dS = dx dy$:

$$I_0(\vec{r}, \lambda, \theta) = 2 \frac{k_0^2}{4\pi^2} \frac{c}{\lambda^2} \sum_{i=1}^p 4\pi \frac{c}{\lambda} \vec{\epsilon}_i \Re \{ \tilde{n}_0 \} \frac{|C'_{0,i-1}|^2 \beta_i^0 \left(\frac{k_0 \sin \theta_0}{2\pi}, \frac{c}{\lambda} \right)}{4|\tilde{n}_i|^2 |\Delta Y_{i-1}|^2} \Theta \left(\frac{2\pi c}{\lambda}, T_i(\vec{r}, z_i) \right) \quad (37)$$

$$I_S(\vec{r}, \lambda, \theta) = 2 \frac{k_s^2}{4\pi^2} \frac{c^2}{\lambda^2} \sum_{i=1}^p 4\pi \frac{c}{\lambda} \vec{\epsilon}_i \Re \{ \tilde{n}_s \} \frac{|C_{i,p}|^2 \beta_i^s \left(\frac{k_s \sin \theta_s}{2\pi}, \frac{c}{\lambda} \right)}{4|\tilde{n}_i|^2 |\Delta Y_i|^2} \Theta \left(\frac{2\pi c}{\lambda}, T_i(\vec{r}, z_i) \right)$$

Recall that the quantities in Expression (27) are relative to an elementary area, necessitating integration over the entire surface of the component (see Eq. (33)). However in most situations approximations can be done for this integration. First we note that the integration term in Eq. (33) can be written as:

$$\int_{\vec{r}} \Theta(2\pi f, T_i(\vec{r}, z_i)) d\vec{r} = S_i \bar{\Theta}(f, z_i) \quad (38)$$

where $\bar{\Theta}$ is the mean of Θ over surface S_i . Then one can consider the fact that the (transverse) thermal radii are most often very close in each layer of the stack, so that the approximation $S_i \approx S$ can be used, and this allows to replace $\Theta_i(f, \vec{r}, z_i)$ by $\bar{\Theta}(f, z_i)$ in (37). Such approximation is not necessary but may allow to strongly reduce the calculation time.

Finally, for each layer if one seeks to obtain a variable independent of temperature, normalization can be proceeded by the (isotropic) black-body spectral intensity at the same average layer temperature, given by $I_b(\lambda, T_i) = 2 \frac{k_0^2}{4\pi^2} \frac{c}{\lambda^2} \Theta \left(\frac{2\pi c}{\lambda}, T_i \right)$, for emission into the superstrate [8,11]. For each layer we thus obtain the emissivity

$$\epsilon_i(\lambda, \theta) = \frac{I_{0i}(\lambda, \theta, T_i)}{I_b(\lambda, T_i)} \quad (39)$$

Due to the presence of the Θ terms in both I_{0i} and I_b , and provided that the average temperature can be used, the temperature does not intervene in (39). In the case where the temperature is essentially the same in each layer, the quantity $\Theta \left(\frac{2\pi c}{\lambda}, T_i \right)$ is constant within the volume of the stack which can then be characterized by an intrinsic overall emissivity. This last emissivity only depends on the multilayer design. Recall that this emissivity for a given pair (λ, θ) is the same as its absorption when subjected to illumination under the same conditions (λ, θ) [8,11].

3. Numerical results for a multi-layer component subjected to various illumination regimes

In this part we use the modeling technique developed in section 2 to calculate the photo-induced thermal radiation of a multi-layer interference filter subjected to a pulsed illumination. To this end we require prior knowledge of the temperature rise $\Delta T(\vec{r}, z, t)$ due to this illumination. This is obtained by completely modeling the photo-induced temperature in an interference filter, as described in a recent article [29]. Since we are mainly interested in temporal, wavelength, angular or depth variations, the numerical calculation will be most often performed for the radiative spectral intensity given in (36-37), at the lateral position $\vec{r} = (0, 0)$ of the component where the temperature is maximum. The impact of the lateral temperature profile, which is less pronounced with these multi-dielectrics in a ns regime, will be addressed in section 3.1.

In what follows we consider optical thin films currently used in the mid-infrared range (MIR), and coatings with an operating point (design wavelength) around $2\mu m$. First we address the

case where the photo-induced temperature rise in the components is small, corresponding to a common domain of application where both optical power densities and absorption levels are low. Under these conditions the filter formula barely affects the thermal radiation blackbody curve whose barycenter is around $10\mu\text{m}$ at room temperature. By contrast, in a second step we shall see, for high rises of the photo-induced temperature, how the spectral behavior of thermal radiation is altered by the multi-layer.

3.1. Mirror with low temperature rise

Consider a MIR multi-dielectric mirror (sometimes described by some within the community as a 1D photonic crystal) comprising 5 quarter wave layers at $\lambda_0 = 2\mu\text{m}$, of formula $H(LH)^2$ and deposited onto a Ge substrate. In the mirror formula, H represents a layer of a high index material (Ge), while L is used for a low index material (BaF_2). The H and L layers have a quarter wavelength optical thickness at the mirror's center wavelength λ_0 , so for illumination at normal incidence [4],

$$n_H e_H = n_L e_L = \frac{\lambda_0}{4} \quad (40)$$

Due to the high index ratio (n_H/n_L) in the MIR range, a small number of layers is sufficient to achieve high reflection ($R \approx 98, 3\%$). The optical and thermal parameters of the media are summarized in Table 1 [44]. Note that Ge and BaF_2 have slight index dispersion in the MIR range, for which reason we use their average index values. These index values (and notably the imaginary index - here taken at 10^{-4} for the thin films) may depend on the deposition conditions and technology. Absorption in the Ge substrate is not considered. Eventually the temperature dependence of all quantities is not considered.

Table 1. Optical and Thermal Parameters Used for the Calculation of Laser-Induced Thermal effects

Materials	BaF2	Ge	Air	Substrate: Ge
Average MIR refractive index	$1.45 + 10^{-4}j$	$4 + 10^{-4}j$	1.	4
Thermal conductivity (W/mK)	11.72	58.61	$2.5 \cdot 10^{-2}$	58.61
Thermal diffusivity (m^2/s)	$58.5 \cdot 10^{-7}$	$354.7 \cdot 10^{-7}$	$2.05 \cdot 10^{-5}$	$354.7 \cdot 10^{-7}$

This MIR component is illuminated by a single laser pulse whose parameters are given in Table 2. The temporal and spatial envelopes of the beam are assumed to be Gaussian, with pulse width τ and illuminated area of radius L . The duration of the laser pulse is set at one nanosecond, and the average illumination wavelength λ is the design wavelength of the coating ($\lambda = \lambda_0 = 2\mu\text{m}$). The process of laser damage that might result from this flux is not considered.

Table 2. Source Parameters

Wavelength	Incident angle	Polarization	Energy	L	τ
$2\mu\text{m}$	0°	TE	1 mJ	$100\mu\text{m}$	1 ns

The photo-induced temperature fields at the center of the beam ($\vec{r} = \vec{0}$) are shown in Fig. 2(a) is the temporal response $\Delta T(z_{max}, t)$ calculated at z_{max} where ΔT is a maximum, and b) is the depth distribution $\Delta T(z, t_{max})$ within the stack calculated at instant t_{max} where ΔT is maximum. The maximum temperature rise obtained is $\Delta T = 9\text{K}$ for these dielectric components of low imaginary index ($n'' = 10^{-4}$). Ordinarily, at these pulse lengths the temperature decay time is much longer than the duration of the laser pulse. Similarly, the spatial distribution of ΔT in this ns regime approaches the envelope of the stationary electric field in the stack [7,45], which explains the higher elevation in the first few layers.

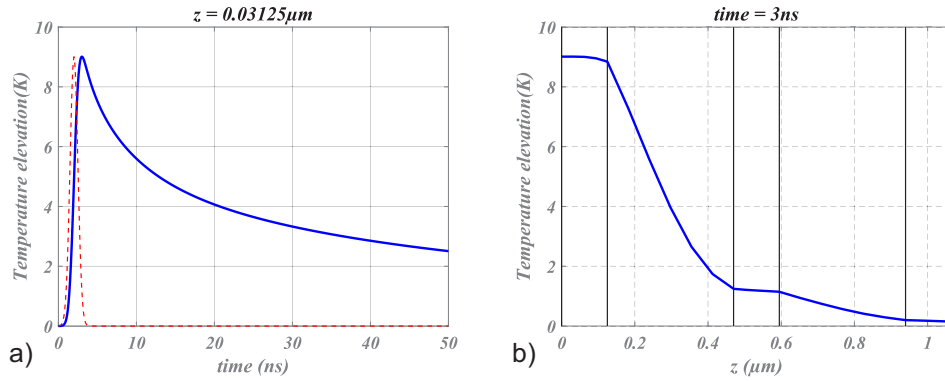


Fig. 2. a) Temporal evolution (blue curve) of the photo-induced temperature rise $\Delta T(z_{max}, t)$ in a quarter-wave mirror illuminated with a ns pulsed laser. Dotted red: temporal evolution of the laser pulse (assumed to be Gaussian) in arbitrary units. b) Spatial distribution of the temperature $\Delta T(z, t_{max})$ in the thickness of the layers, with the substrate at the right side.

The radiative spectral intensity is then calculated from the temperature field of Fig. 2, increased by an ambient temperature of 20°C. This is calculated at the center of the beam ($\vec{r} = \vec{0}$). In order to apply Eq. (30), the layers have been subdivided into thin sub-layers on account of the rapid variations of ΔT in each layer of the component (see Fig. 2). The resulting temporal variation of the radiative spectral intensity is shown in Fig. 3(a). This is calculated at direction $\theta_0 = 0^\circ$ at the wavelength corresponding to the maximum thermal emission ($\lambda = 8.73 \mu\text{m}$). Figure 3(b) plots the spectral intensity as a function of the emission wavelength, still at $\theta_0 = 0^\circ$. Figure 3(c) plots the spectral intensity as a function of the angle of emission in the superstrate at $\lambda = 7.7 \mu\text{m}$. On these two curves (Fig. 3(b) and (Fig. 3(c)), the blue curve represents the radiative intensity with the component at ambient temperature, shown by a blue dot on the temporal curve given in Fig. 3(a); the red curve corresponds to the instant at which the intensity is a maximum, shown by the red dot on the temporal curve in Fig. 3(a).

Several conclusions can be drawn from Fig. 3. Firstly, the levels of spectral intensity are low on account of the low absorptivity of dielectric materials that induce low emissivity. Secondly, apart from this low level of intensity, the radiative spectral and angular curves are similar to those of a black body (apart from slight curvature beyond $4 \mu\text{m}$). Actually the effect of the filter is expected essentially in the vicinity of its design wavelength ($2 \mu\text{m}$) in the near infra-red (NIR), but the radiation in this spectral domain is weak compared with that of the mid infra-red (MIR, $8 \mu\text{m}$) on account of the low rise in temperature.

Hence, in order to observe the effect of the filter formula on the black body radiation, we must either use a mirror centered around $8 \mu\text{m}$, or increase ΔT to shift the radiation to shorter wavelengths ($2 \mu\text{m}$). It is this latter case that is assumed in section 3.2.

As a reminder, all curves in Fig. 3 are calculated at the center $\vec{r} = (0, 0)$ of the emissive surface where the temperature is maximum. As for the impact of the lateral temperature profile, it is highlighted in Fig. 4, where the radiative spectral intensity is plotted versus the lateral dimension of the component. The numerical data are given at the time, wavelength and angle at which the temperature is maximum. Recall that the laser is gaussian with a spot size of $100 \mu\text{m} * 100 \mu\text{m}$. As expected, the lateral behavior is very close to that of the function of $\Theta\left(\frac{2\pi c}{\lambda}, T_i(\vec{r}, z_i)\right)$ given in Eq. (37), which is nearly the same in the depth of the multilayer in a ns regime. Note that this behavior will be less pronounced when the flux of Eq. (33) is calculated, since this flux is proportional to the integral of the Θ function.

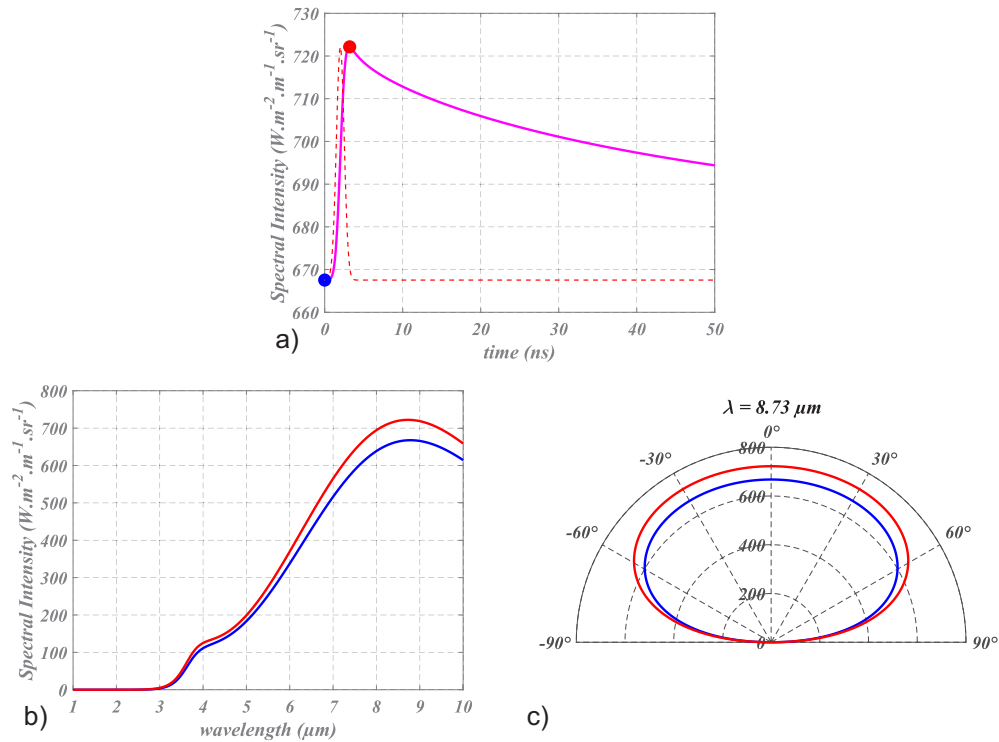


Fig. 3. Spectral intensity of the thermal radiation of the quarter-wave mirror of Fig. 2 subjected to a (1 ns, 1mJ) pulsed laser. a) temporal evolution at normal emission angle and $\lambda = 7.7 \mu m$. b) spectral variation at normal emission angle. c) angular variation at $\lambda = 7.7 \mu m$. The red and blue curves are calculated respectively at the instants given by the red and blue dots of figure a).

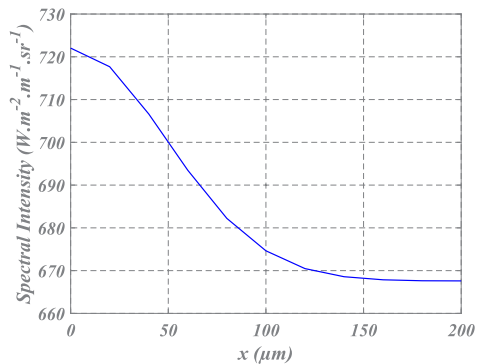


Fig. 4. Radiative spectral intensity of the quarter-wave mirror of Fig. 3, calculated versus the transverse dimension of the component (see text).

3.2. Mirror with pronounced temperature rise

The filter function should therefore have a gradual effect on the radiation as the temperature rises. Since this phenomenon is proportional to the energy of the laser beam, we now consider the same ns laser pulse from Fig. 2, but with an energy of 150 mJ. Note that the damage process due to the laser flux [7] is not taken into account, since we are only interested in verifying the radiation model.

Figure 5(a) plots the radiative spectral intensity of the mirror studied in section 3.1 as a function of wavelength. The direction is $\theta_0 = 0^\circ$ and the curves are calculated at different points in time for which the maximum temperature elevation inside the mirror is given. All curves are normalized by their maximum value in order to be visible on the same graph.

As expected, we observe that the radiation spectrum shifts to short wavelengths and departs significantly from the black body emission curve as a result of the interference filtering in the NIR region due to the multi-layer. This result illustrates the effect of the multilayer in the thermal radiation process. Visualization 1 shows the dynamic of the process without normalization.

To be complete, the mirror emissivity is plotted in Fig. 5(b). The curve presents two significant peaks in the NIR region [1 μm - 2 μm] and small variations at larger wavelengths. Consequently, the emission of the mirror deviates significantly from that of the blackbody when its maximum emission is in the NIR, thus when the temperature is higher than 1450 K (according to Wien's law). This explains the 2 peaks of the pink curve in Fig. 5(a) (corresponding to a temperature of 1645 K).

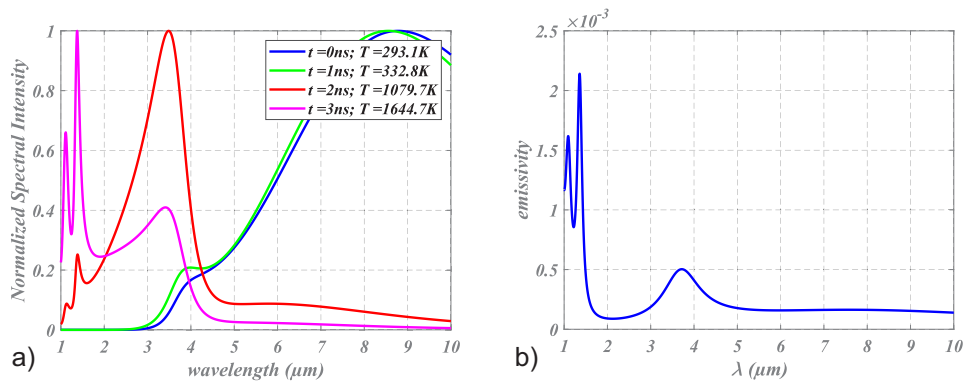


Fig. 5. a) Spectral intensity versus wavelength of thermal radiation from the quarter-wave mirror of Fig. 2 subjected to a ns pulsed laser, for different pulsed energies (1mJ, 50 mJ, 100 mJ and 150 mJ). The curves are normalized by their maximum value (see Visualization 1 without normalization). b) emissivity of the mirror.

4. Narrow-band enhancement of thermal radiation

We have just seen that the filter function of a multi-layer component can significantly alter its thermal radiation, provided the emission wavelength is close to the center wavelength of the filter. In this part we shall turn our attention to how filters can be designed to confine and enhance thermal radiation. A desire to tailor the thermal radiation has led to the design and manufacture of many structures in the literature [10]. For example, 2D multi-layer structures [20] can be mentioned, gratings [14], meta-surfaces [21] or 1D structures such as metal Fabry-Perot filter [11], photonic crystals coated with SiC [13] or Ag [12] and Bragg stacks [46]. Huge works have also been made in controlling thermal radiation in energy saving related domain [18,19]. To a greater or lesser degree, all these components confine the thermal radiation in an angular or spectral sense.

For this application we shall draw on work already carried out in the domain of luminescent micro-cavities, where sources are also described by surface or bulk electric currents [4,36,37,43]. Much work has been devoted to controlling the radiation of an arbitrary surface current located in a planar multi-layer structure [36,37]. We have recently shown how a particular structure containing a ZAL (zero admittance layer, [40]) layer can generate a strong enhancement (or inhibition) of the field radiated by an electric current located within the structure [43]. The question therefore arises as to whether the same effects can be obtained to cause the thermal radiation to be enhanced or inhibited.

As mentioned in the introduction, and because we have adopted an approach based on spatio-frequency wave packets using the method of complex admittances, our thermal radiation modeling process is similar to that for micro-cavities, with two major differences. On the one hand, the analytical expression for the currents is very different, while on the other hand, the radiation currents are bulk currents (in contrast with the surface cavity currents that enabled ZAL layers to be tested). Despite these differences, we observe that the admittance difference ΔY appears in Eq. (3) and we know that the poles of this quantity control how the ZAL layers work. Moreover, we also know that bulk currents can be reduced to surface currents [47]. These remarks indicate that the same effects should be obtained to confine thermal radiation, what we shall verify in due course.

Hence, we consider a multi-layer MIR component in which a multi-dielectric mirror centered around $2\mu\text{m}$ is associated with a ZAL layer. Thin film materials are still G_e and BaF_2 , but G_e is now the superstrate from which the illumination comes, while the substrate is air [40]. Recall [40] that the mirror is designed to work at oblique incidence θ_0^0 in the superstrate, and is therefore matched as

$$n_H e_H \cos \theta_H^0 = n_L e_L \cos \theta_L^0 = \frac{\lambda^0}{4} = 2\mu\text{m} \quad (41)$$

with θ_H^0, θ_L^0 the angles within the H and L materials. As mentioned above, the index ratio n_H/n_L in the MIR range is high with these materials, so that a few layers is enough to reach a high reflection, all the more than oblique incidence is used. The final structure for incidence θ_0^0 is therefore $G_e/LHL/ZAL/Air$. The ZAL layer is made of BaF_2 and determined to obtain a thermal radiation enhancement in S polarization at $(\lambda^0, \theta_0^0) = (2\mu\text{m}, 20^\circ)$, giving a thickness of 725.76 nm.

4.1. Static case at ambient temperature

Though we are interested in a pulsed photo-induced regime (see section 4.2), we start with the case of a coating at ambient temperature. Indeed following Eq. (39) and related assumptions, the multilayer emissivity is not temperature dependent, so that it will not vary with time in a pulsed regime. Therefore, the coating emissivity (which is an intrinsic property of the multilayer) can be investigated regardless of the regime. We analyze below the component's ability to confine thermal radiation.

In a first step we plot in Fig. 6 the result in terms of spectral emissivity at ambient temperature. Figure 6(a) shows the emissivity as a function of the angle of emission, and Fig. 6(b) shows the emissivity as a function of wavelength. As expected, the thermal radiation is very strongly confined about the pair $(\lambda^0 = 2\mu\text{m}, \theta_0^0 = 20^\circ)$ with an emissivity close to 1; this is despite the low imaginary index of the layers ($n'' = 10^{-4}$), on account of the great enhancement of the electric field produced by the ZAL layer [40]. Therefore, as for the micro-cavity case [43], the radiation is enhanced by a factor close to 10^4 . More precisely, the structure radiates thermally for all pairs (λ, θ_0) of the line shown in Fig. 6(c). Finally, Fig. 6(d) plots the change in spectral emissivity at (λ^0, θ_0^0) as a function of the number of layers of the multi-dielectric mirror. The greatest emissivity (3 layers) is that we used in this section. The low layer number (3) results from the high index ratio in the MIR.

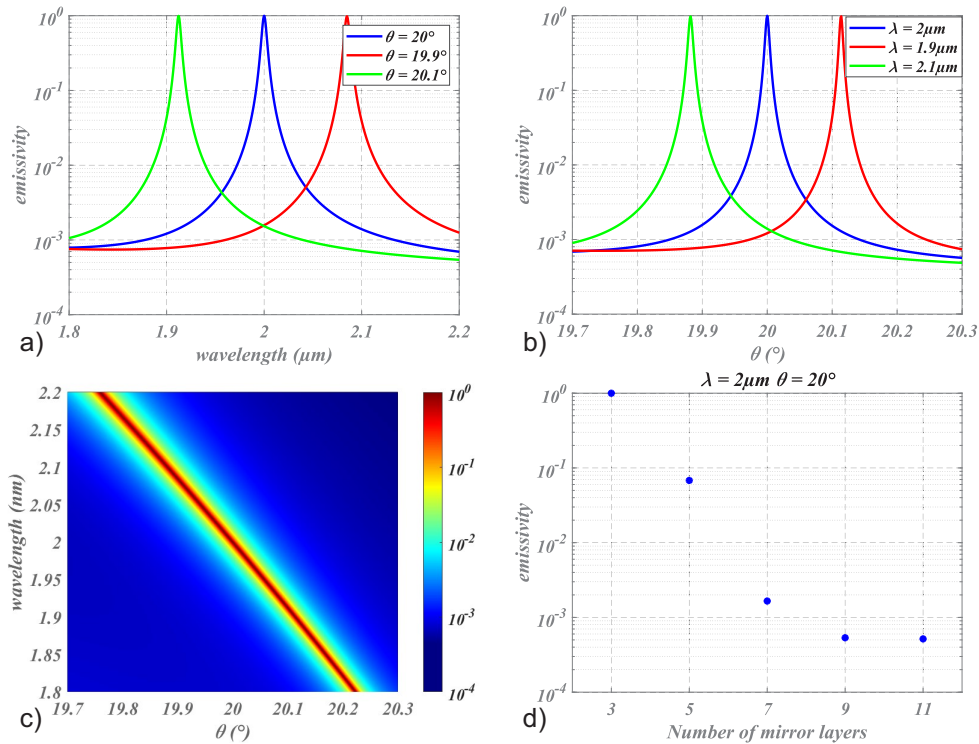


Fig. 6. Spectral emissivity for a ZAL structure. Emissivity with respect to wavelength at 3 angles a), emissivity with respect to emission angle at 3 wavelengths b) and emissivity with respect to both c). Maximum emissivity with respect to the number of layers of the mirror d).

To allow comparison with the results in the literature, the spectral $\Delta\lambda$ and angular $\Delta\theta$ bandwidths at half the emissivity maximum are calculated. We find $\Delta\lambda = 5.6 \text{ nm}$, giving a quality factor in the MIR (as defined in [10]) of $Q = \lambda^0 / \Delta\lambda = 356$. We also have $\Delta\theta = 0.006^\circ$, which defines a spatial coherence $L_c = \frac{1}{\Delta\theta} \lambda^0 = 9554 \lambda^0$. The quality factor and coherence length are thus similar to those of the structures described in [10,12–14]. Reference [48] demonstrates a resonant cavity coupled with a greater spatial coherence and resonance factor.

4.2. Dynamic case: photo-induced thermal radiation

We now consider a photo-induced situation and analyze thermal radiation. The heat source comes from the absorption of the coating illuminated in a single pulse regime. Unlike the emissivity, thermal radiation (ThR) is temperature dependent, and so is time dependent. The ThR shaping by the ZAL coating will be more pronounced when the adequate temperature is reached at some point in time where the blackbody wavelength of maximum energy is not too far from the operation point of the coating ($2 \mu\text{m}$).

We use the ms regime to ensure that all layers support a significant heat source. Indeed in this regime the temperature does not follow the electromagnetic field within the multilayer, so that the heat source is quasi-uniform within the coating. Such condition is necessary to optimize the coating efficiency. For shorter duration pulses, the temperature follows the stationary optical field and it would be necessary to check the temperature level in the ZAL layer.

In order to limit the incident power, the coating is illuminated at its resonance frequency $(\lambda, \theta_0) = (\lambda^0, \theta_0^0) = (2 \mu\text{m}, 20^\circ)$ in S polarization. Due to the enhancement of the evanescent field within the stack, absorption is highly increased and the resulting temperature elevation,

with a 5mJ laser pulse of 1 ms, is greater. We find $\Delta T = 257K$, a value to be compared to 0.18 K outside the resonance wavelength.

The results are shown in Fig. 7, which emphasizes the narrow peak of thermal radiation at $2\mu m$. Figure 7(a) is given for the thermal radiation versus time, at wavelengths and angles given by $(\lambda = \lambda^0 = 2\mu m, \theta_0 = \theta_0^0 = 20^\circ)$. Figure 7(b) is given for the wavelength spectrum of the thermal radiation, at two different times. The blue curve is calculated at instant 0 where the temperature is the ambient temperature (293 K), while the red curve is calculated at the instant where the temperature rise is maximum (see the blue and red dots on Fig. 7(a)). The dynamic behavior that results from Fig. 7(b) can be seen in Visualization 2.

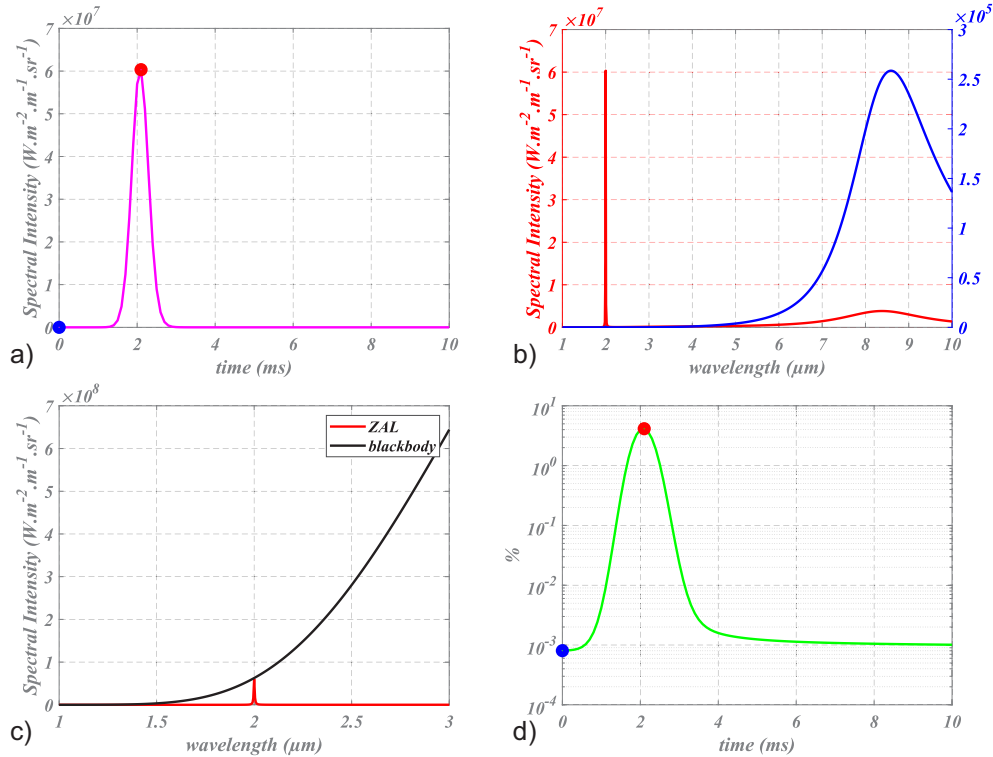


Fig. 7. Spectral intensity (ThR) plotted for the ZAL coating illuminated with a single pulse laser (1 ms, 5mJ, $2\mu m$, 20°). a: ThR is plotted versus time at wavelength $2\mu m$ and direction 20° . b: ThR at direction 20° is plotted in blue at ambient temperature (time = 0, see blue dot in a) and plotted in red at time where the maximum temperature is reached (see red dot in the a). c) Th R is plotted in red at time where the maximum temperature is reached and compared with blackbody intensity at same temperature. d) integral of the ThR over a 20 nm bandwidth around $2 \mu m$ and normalized by the integral of ThR over the entire spectrum [1 -10 μm].

To be complete, we provide in Fig. 7(c) a comparison between the spectral intensities of the ZAL structure and the blackbody at the same temperature. The temperature (550 K) is the sum of the ambient and photo-induced temperatures. As expected, both intensities are equal at $2 \mu m$ where the emissivity is unity.

As seen in Fig. 7(b) and in Visualization 2, the thermal radiation is progressively confined and enhanced around the resonance at $2 \mu m$. For more detail, the integral of the spectral intensity over a 20 nm bandwidth around $2 \mu m$ is plotted as a function of time in Fig. 7(d). This integral is normalized by the integral in the range [1 μm - 10 μm] and expressed as a percentage. As shown

in Fig. 7(d), at the maximum temperature elevation (red dot), the resonance accounts for 4% of the thermal radiation in the range [1 μm - 10 μm], while at ambient temperature (blue dot) it accounts 0.0008%.

We should keep in mind that the efficiency of the ZAL coating can be reduced in practice, depending on the manufacturing precision of the multi-layer. Finally, the ZAL structure can be optimized at any wavelength; choosing $\lambda^0 = 10\mu\text{m}$ would lead to a confinement at ambient temperature. In conclusion, planar structures based on ZAL layers offer a complementary alternative in shaping thermal radiation in predefined narrow-band windows.

5. Conclusion

We have presented an electromagnetic model that, in a very general case, calculates the photo-induced transient thermal radiation in interference filters as functions of the illumination parameters of the coating (energy, pulse duration, spot size, incidence and polarization). Radiation sources were introduced into Maxwell's equations using the fluctuation-dissipation theorem [9,10,34], taking into account the spatio-temporal variation of the photo-induced temperature [29]. Pulse lengths are in the order of a nanosecond, large enough to allow thermalization process to take place. The method of solution is based on our previous work covering bulk scattering [35] and luminescent micro-cavities [36,37,43], drawing on electromagnetic optics [4]. The statistical phase properties of thermal currents were used to simplify the equations.

We considered 3 variables: flux per unit solid angle, radiative spectral intensity, and emissivity. Numerical results allowed us to plot thermal radiation curves as functions of time, wavelength, emission angle and position at the emissive surface. Various structures were analyzed. For multi-dielectric mirrors in the MIR we were able to show how the filter formula affects the radiation it emits, this being very different from that of a black body at the same temperature. We also showed how ZAL structures [40] enable the radiation to be intensely confined at predefined frequencies, in angle and wavelength, with an emissivity close to unity.

We believe this work can be useful for the optical thin film community. In particular, it could help to design multilayers to control thermal radiation, drawing on already well-established thin film design techniques [4]. Note also that we used a direct method to calculate the thermal radiation, in particular because our method can be extended to take account of the energy density stored in the evanescent waves, that can be decoupled by an optical tunnel effect [38], and which takes part in the energy balance for dissipative media [4]. Above all, this model will allow to quantify the amount of radiation transferred to the many guided modes of the multi-layer structure [39], which will be covered in a forthcoming publication.

Acknowledgment. We acknowledge the joint laboratory (LabTop) which gathers CILAS and Institut Fresnel, and the Centre National d'Etudes Spatiales (CNES), for their support. We acknowledge Karl Joulain and Jean-Jacques Greffet for helpful discussions about the area of validity of the fluctuation dissipation theorem.

Disclosures. The authors declare no conflicts of interest.

Data availability. No data were generated or analyzed in the presented research.

Supplemental document. See [Supplement 1](#) for supporting content.

References

1. H. A. Macleod, *Thin-Film Optical Filters*, 4th ed, Series in *Optics and Optoelectronics* (CRC Press/Taylor & Francis, 2010).
2. P. W. Baumeister, *Optical Coating Technology* (SPIE Press, 2004).
3. N. Kaiser and H. K. Pulker, eds., *Optical Interference Coatings, Springer Series in Optical Sciences* (Springer, 2003).
4. C. Amra, M. Lequime, and M. Zerrad, *Electromagnetic Optics of Thin-Film Coatings: Light Scattering, Giant Field Enhancement, and Planar Microcavities* (Cambridge University Press, 2021).
5. B. Canuel, E. Genin, and G. Vajente, *et al.*, "Displacement noise from back scattering and specular reflection of input optics in advanced gravitational wave detectors," *Opt. Express* **21**(9), 10546 (2013).
6. I. Khan, M. Lequime, and M. Zerrad, *et al.*, "Detection of Ultralow Light Power Back-Reflected or Back-Scattered by Optical Components Using Balanced Low-Coherence Interferometry," *Phys. Rev. Appl.* **16**(4), 044055 (2021).

7. D. Ristau, *Laser-Induced Damage in Optical Materials* (CRC Press, 2015).
8. John R. Howell, M. Pinar Mengüç, and Robert Siegel, *Thermal Radiation Heat Transfer*, 6th ed. (CRC Press, 2016).
9. S. M. Rytov, Yu. A. Kravtsov, and V. I. Tatarskii, *Principles of Statistical Radiophysics 3: Elements of Random Fields* (Springer-Verlag, 1989).
10. Z. M. Zhang, *Nano/Microscale Heat Transfer*, 2nd ed., Mechanical Engineering Series (Springer International Publishing, 2020).
11. L. P. Wang, S. Basu, and Z. M. Zhang, "Direct and indirect methods for calculating thermal emission from layered structures with nonuniform temperatures," *J. Heat Transf.* **133**(7), 1 (2011).
12. B. J. Lee, Y.-B. Chen, and Z. M. Zhang, "Surface waves between metallic films and truncated photonic crystals observed with reflectance spectroscopy," *Opt. Lett.* **33**(3), 204–206 (2008).
13. B. J. Lee and Z. M. Zhang, "Coherent thermal emission from modified periodic multilayer structures," *J. Heat Transf.* **129**(1), 17–26 (2007).
14. J.-J. Greffet, R. Carminati, and K. Joulain, *et al.*, "Coherent emission of light by thermal sources," *Nature* **416**(6876), 61–64 (2002).
15. S. Buddhiraju, W. Li, and S. Fan, "Photonic Refrigeration from Time-Modulated Thermal Emission," *Phys. Rev. Lett.* **124**(7), 077402 (2020).
16. A. Narayanaswamy and G. Chen, "Thermal emission control with one-dimensional metalodielectric photonic crystals," *Phys. Rev. B* **70**(12), 125101 (2004).
17. M. Francoeur, M. Pinar Mengüç, and R. Vaillon, "Solution of near-field thermal radiation in one-dimensional layered media using dyadic Green's functions and the scattering matrix method," *J. Quant. Spectrosc. Radiat. Transf.* **110**(18), 2002–2018 (2009).
18. P. Bermel, J. Lee, and J. D. Joannopoulos, *et al.*, "Selective solar absorbers," *Annu. Rev. Heat Transf.* **15**(15), 231–254 (2012).
19. K.-T. Lin, J. Han, and K. Li, *et al.*, "Radiative cooling: Fundamental physics, atmospheric influences, materials and structural engineering, applications and beyond," *Nano Energy* **80**, 105517 (2021).
20. B. Zhao, L. Wang, and Y. Shuai, *et al.*, "Thermophotovoltaic emitters based on a two-dimensional grating/thin-film nanostructure," *Int. J. Heat Mass Transf.* **67**, 637–645 (2013).
21. X. Liu, T. Tyler, and T. Starr, *et al.*, "Taming the Blackbody with Infrared Metamaterials as Selective Thermal Emitters," *Phys. Rev. Lett.* **107**(4), 045901 (2011).
22. P. N. Dyachenko, S. Molesky, and A. Y. Petrov, *et al.*, "Controlling thermal emission with refractory epsilon-near-zero metamaterials via topological transitions," *Nat. Commun.* **7**(1), 11809 (2016).
23. A. P. Raman, M. A. Anoma, and L. Zhu, *et al.*, "Passive radiative cooling below ambient air temperature under direct sunlight," *Nature* **515**(7528), 540–544 (2014).
24. W. Li, Y. Shi, and K. Chen, *et al.*, "A Comprehensive Photonic Approach for Solar Cell Cooling," *ACS Photonics* **4**(4), 774–782 (2017).
25. J. Xu, J. Mandal, and A. P. Raman, "Broadband directional control of thermal emission," (n.d.).
26. Y. Zhu, H. Luo, and C. Yang, *et al.*, "Color-preserving passive radiative cooling for an actively temperature-regulated enclosure," *Light: Sci. Appl.* **11**(1), 122 (2022).
27. C. Petite, R. Marcouillé, and A. Moreau, *et al.*, "Multipass lock-in thermography for the study of optical coating absorption," *Appl. Opt.* **61**(4), 978 (2022).
28. S. I. Maslovski, C. R. Simovski, and S. A. Tretyakov, "Equivalent circuit model of radiative heat transfer," *Phys. Rev. B* **87**(15), 155124 (2013).
29. P. Rouquette, C. Amra, and M. Zerrad, *et al.*, "Photo-induced Temperature in Optical Interference Coatings," *Opt. Express* **30**(26), 46575–46601 (2022).
30. J.-J. Greffet, P. Bouchon, and G. Brucoli, *et al.*, "Light Emission by Nonequilibrium Bodies: Local Kirchhoff Law," *Phys. Rev. X* **8**(2), 021008 (2018).
31. C. Luo, A. Narayanaswamy, and G. Chen, *et al.*, "Thermal Radiation from Photonic Crystals: A Direct Calculation," *Phys. Rev. Lett.* **93**(21), 213905 (2004).
32. D. L. C. Chan, M. Soljačić, and J. D. Joannopoulos, "Direct calculation of thermal emission for three-dimensionally periodic photonic crystal slabs," *Phys. Rev. E* **74**(3), 036615 (2006).
33. C. Amra, D. Petiteau, and M. Zerrad, *et al.*, "Analogies between optical propagation and heat diffusion: applications to microcavities, gratings and cloaks," *Proc. R. Soc. A.* **471**(2183), 20150143 (2015).
34. L. Novotny and B. Hecht, *Principles of Nano-Optics*, 2nd ed. (Cambridge University Press, 2012).
35. C. Amra, "First-order vector theory of bulk scattering in optical multilayers," *J. Opt. Soc. Am. A* **10**(2), 365–374 (1993).
36. C. Amra and S. Maure, "Electromagnetic power provided by sources within multilayer optics: free-space and modal patterns," *J. Opt. Soc. Am. A* **14**(11), 3102–3113 (1997).
37. C. Amra and S. Maure, "Mutual coherence and conical pattern of sources optimally excited within multilayer optics," *J. Opt. Soc. Am. A* **14**(11), 3114–3124 (1997).
38. K. Joulain, P. Ben-Abdallah, and P.-O. Chapuis, *et al.*, "Strong tip-sample coupling in thermal radiation scanning tunneling microscopy," *J. Quant. Spectrosc. Radiat. Transf.* **136**, 1–15 (2014).
39. C. Amra, M. Zerrad, and M. Lequime, "Trapped light scattering within optical coatings: a multilayer roughness-coupling process," *Opt. Express* **29**(16), 25570–25592 (2021).

40. C. Amra, M. Zerrad, and F. Lemarchand, *et al.*, “Energy density engineering via zero-admittance domains in all-dielectric stratified materials,” *Phys. Rev. A* **97**(2), 023819 (2018).
41. L. D. Landau and E. M. Lifshitz, *Statistical Physics: Volume 5*, 3. ed., repr, Course of Theoretical Physics (Elsevier, 2013).
42. S. Volz and R. Carminati, eds., *Microscale and Nanoscale Heat Transfer, Topics in Applied Physics* (Springer, 2007).
43. P. Rouquette, C. Amra, and M. Zerrad, *et al.*, “Micro-cavity optimization for ultra-sensitive all-dielectric optical sensors,” *Opt. Express* **30**(9), 15344–15364 (2022).
44. “crystran,” <https://www.crystran.co.uk/optical-materials>.
45. H. Li, Z. Shen, and X. Ni, “Temperature field analysis of high reflection film induced by long-pulse and short-pulse lasers under different irradiation angles,” *Optik* **126**(23), 4254–4258 (2015).
46. P. Ben-Abdallah and B. Ni, “Single-defect Bragg stacks for high-power narrow-band thermal emission,” *J. Appl. Phys.* **97**(10), 104910 (2005).
47. C. Amra, C. Grèzes-Besset, and L. Bruel, “Comparison of surface and bulk scattering in optical multilayers,” *Appl. Opt.* **32**(28), 5492 (1993).
48. N. Dahan, A. Niv, and G. Biener, *et al.*, “Extraordinary Coherent Thermal Emission From SiC Due to Coupled Resonant Cavities,” *J. Heat Transf.* **130**(11), 112401 (2008).